Dissociative Adsorption of Hydrogen Molecule on Aluminum Clusters: Effect of Charge and Doping

David J. Henry* and Irene Yarovsky*

Applied Sciences, RMIT University, GPO Box 2476V, Victoria, 3001, Australia

Received: October 30, 2008; Revised Manuscript Received: January 12, 2009

The dissociative chemisorption of molecular hydrogen on charged and neutral aluminum clusters $Al_{12}X$ (X = Mg, Al, Si) was investigated using DFT and a modified G3(MP2)-RAD procedure. Reaction barriers and enthalpies were determined for both neutral and singly charged clusters. The lowest barrier for dissociative adsorption of H_2 on a neutral cluster was found for the $Al_{12}Mg$ cluster, whereas the highest barrier was found to be on the closed-shell $Al_{12}Si$. The interaction of H_2 with Al_{13}^+ is found to proceed via an association complex that is 0.07 eV lower in energy than the isolated species and from which the barrier to H_2 dissociative adsorption is only 0.16 eV. The most exothermic reaction of H_2 with $Al_{12}X$ occurs for the Al_{13}^+/H_2 system. In comparison, reactions with the closed-shell Al_{13}^- and $Al_{12}Si$ clusters are found to be endothermic. The barriers for H_2 desorption from the dihydrogenated clusters are generally quite substantial.

1. Introduction

There has been considerable interest in the interaction of hydrogen with light metals in order to discover inexpensive lightweight materials for hydrogen storage. For this to be successful, the interaction of hydrogen with the material must be thermodynamically and kinetically favorable. This means that the barrier for dissociative adsorption of H_2 onto the materials should be relatively low and the binding of hydrogen to the material should be only slightly exothermic.

Alane (AlH_3) and dialane (Al_2H_6) are stable molecules with high hydrogen content (10.07 wt %). Thermodynamics indicate that alane easily decomposes at normal conditions;[1] however, rehydrogenation occurs only at extremely high pressures,[2] which is in accord with theoretical[3,4,5] and experimental[6] studies that indicate that aluminum is a poor metal surface for dissociative adsorption of H_2. Alanates ($M_x(AlH_4)_y$) offer the advantage of improved stability over alane and generally dissociate into the metal hydride (MH), aluminum, and H_2; however, rehydrogenation is also often difficult.[7] Bogdanovic and Schwickardi[8] demonstrated that doping alkali metal hydrides with a few mol % of Ti can lead to reversible decomposition at reasonable temperatures and pressures. Theoretical studies[9,10] of Ti-doped $NaAlH_4$ indicate that the Ti dopant is responsible for catalyzing H_2 chemisorption by altering the electrostatic field at the defect site when the Ti atoms are in specific local arrangements. However, the cyclable hydrogen content of these materials is low (~4%). The challenge therefore remains to combine high hydrogen content with favorable kinetics for adsorption and desorption of H_2.

One possible alternative to these bulk materials is cluster-based materials. The reactivity, electrostatic fields, and surface features of small metal clusters can differ significantly from those of bulk materials and are often dependent on not only the composition but the size of the clusters. Clearly, for many applications the stability of the cluster is also of practical importance. Experimental and theoretical studies have shown that among the small aluminum clusters, Al_7 and Al_{13} are particularly stable[11−14] because their valence electronic configurations approach closed-shell magic configurations, as characterized by the jellium model.[15,16] It has also been proposed that adsorption of hydrogen on Al_{13} can provide the necessary electron to complete its electronic configuration, and therefore $Al_{13}H$ may be suitable for the preparation of new cluster-assembled materials.[17−22] Moreover, Al_{13} and derivatives have been theoretically demonstrated to strongly bond significant numbers of hydrogen atoms ($Al_{13}H_{13}$ and $Al_{12}H_{20}$).[22,23]

Whereas the interaction of the hydrogen atom with aluminum clusters is thermodynamically favored, experimental studies have suggested that the kinetics for chemisorption of the hydrogen molecule on pure aluminum clusters are less favorable. Cox et al.[13] found that chemisorption of D_2 on neutral Al clusters is relatively slow and strongly size specific, with only Al_6 and Al_7 exhibiting significant reactivity. Upton and co-workers[24,25] theoretically investigated the interaction of H_2 with Al_6 and found that although electron transfer from the highest occupied molecular orbital (HOMO) of the cluster to the σ^* orbital of H_2 plays a role in weakening the H−H bond that this may not be the most important factor determining the height of the activation barrier. In conjunction with this specific interaction, significant changes in the cluster populations are necessary to initially minimize repulsive interactions between the cluster and H_2 and then subsequently enable formation of the new Al−H bonds. Jarrold and Bower[26] studied chemical reactions between Al_n^+ ($n = 3 - 27$) and D_2 as well as chemisorption of deuterium to give metastable $Al_nD_2^+$ adducts, using low-energy ion beam techniques. For Al_{12}^+ and the larger clusters, the main reaction product was generally Al_nD^+ with smaller amounts of $Al_{n-1}D^+$. Significantly, they found that $Al_nD_2^+$ adduct formation occurred in the ion beam for all clusters in the size range of Al_8^+ to Al_{27}^+, except for Al_{13}^+, and that these adducts arise from single collisions. However, their results indicate that the activation barriers for chemisorption on Al_n cluster ions with $n = 10-27$ are quite high, such that the rate constants at room temperature are effectively zero. Cui et al.[27] investigated $Al_nD_2^-$ ($n = 3, 6-15$) anions using photoelectron spectroscopy, which was able to reveal the nature of the interaction between D_2 and the Al_n^- cluster. Their results suggest that for the closed-shell Al_n^- ($n = 9$, 11, 13, and 15), D_2 is physisorbed on the clusters, whereas

* To whom correspondence should be addressed. E-mail: david.henry@rmit.edu.au (D.J.H.),irene.yarovsky@rmit.edu.au (I.Y.).

10.1021/jp809619q CCC: $40.75
Published on Web 02/18/2009

for the open-shell Al_n^- (n = 8, 12, and 14) the spectra suggest that D_2 is chemisorbed on the clusters. In comparison, for $Al_nD_2^-$ (n = 3, 6, 7, and 10), completely different spectra are obtained, which suggest that D_2 is dissociatively adsorbed onto the clusters. These results clearly demonstrate the size and charge dependence of reactivity of small aluminum clusters, which relates directly to the total number of valence electrons for the cluster.

It is therefore of interest to investigate theoretically what factors contribute to the slow kinetics for dissociative hydrogen adsorption on pure aluminum clusters, in particular Al_{13}, and to determine what effects charge and the presence of dopants (Mg, Si) have on the reaction barriers and thermodynamics. In this study, we investigate the interaction of molecular hydrogen with a series of neutral and charged aluminum clusters ($Al_{12}X^z$, X = Mg, Al, Si, and $z = -1, 0, +1$) using DFT and a modified form of the high-level G3(MP2)-RAD procedure.

2. Computational Procedures. Standard DFT and ab initio calculations[28,29] were performed using the *DMol*^{3},[30] *Gaussian 03*,[31] and *MOLPRO*[32] computer programs. All geometries were calculated with the PBE functional[33] using the double numerical-polarized (DNP) and 6-311G(d,p) basis sets. Both of these basis sets include a *d*-type polarization function on heavy atoms and a *p*-type polarization function on hydrogen. It was previously shown that an all electron basis set with the addition of *d* functions is essential for a proper description of high-valence Al atoms.[34] The computationally economical DNP basis set is comparable in size to the Gaussian-type 6-31G(d,p) basis set and has been found to give similar performance for Al cluster geometries and binding energies.[35]

In all *DMol*^{3} calculations, atom centered grids were used for the numerical integration with the Fine option that includes about 2000 grid points for each atom. The real space cutoff of 10.0 Å was imposed for numerical integration. Self-consistent-field (SCF) convergence criterion was set to the rms change in the electronic density to be less than 2.7×10^{-5} eV. The convergence criteria applied for geometry optimization were 2.7×10^{-4} eV for energy, 0.054 eV/Å for force, and 0.005 Å for displacement. The thermal occupation option in *DMol*^{3}, which uses a finite-temperature Fermi function to compute fractional occupations by mixing virtual orbitals into the occupied space, is often necessary to achieve SCF convergence in metallic systems. Therefore, we have assessed the performance for the neutral systems using both standard Fermi occupations (PBE/DNP) and the thermal occupation level set at 0.136 eV (PBE/DNP(Thermal)).

Vibrational frequency analysis was performed to characterize all stationary points reported here as true minima or transition structures. Intrinsic reaction coordinate (IRC) calculations were performed to confirm that all transition structures were truly linked to the corresponding reactant and products. All energies determined in the present study have been corrected for zero-point vibrational energy.

Reaction barriers and enthalpies were evaluated at each level used for geometry optimization and compared with benchmark values obtained with a modified form of the high-level G3(MP2)-RAD procedure.[36] Modifications in the present study include the use of PBE/6-311G(d,p) geometries and unscaled PBE/6-311G(d,p) zero-point vibrational energy corrections. Partial atomic charges were determined using the atomic polar tensors approach of Cioslowski.[37]

3. Results and Discussion

A. Assessment of Procedures for Transition-State Structures and Reaction Energies. Recently,[35] we assessed the performance of DNP, 6-31G(d,p), and 6-311G(d,p) basis sets with the PBE and PW91 functionals for the evaluation of geometries and energies of Al_{13} and $Al_{12}Si$ clusters, their cations, anions, and mono- and dihydrides. We found that PBE/6-311G(d,p) gave very close agreement with the benchmark CCSD/6-31G(d,p) level for ground-state geometries and provides a suitable secondary benchmark level. The economical PBE/DNP level also gave good performance against the CCSD/6-31G(d,p) level and provides a suitable alternative to more computationally expensive procedures.

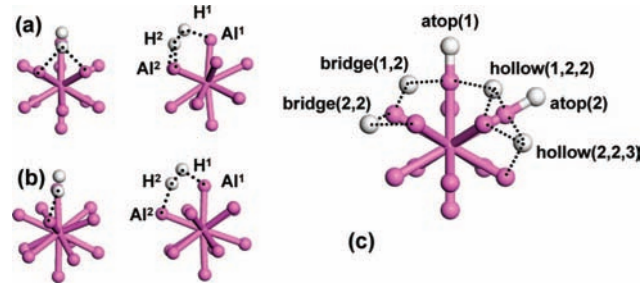

Figure 1. Front and side views of (a) hollow and (b) bridge transition structures. (c) Definitions of H adsorption sites on $Al_{12}XH_2$ clusters.

TABLE 1: Geometric Parameters of $Al_{12}X/H_2$ (X = Al, Si, Mg) Transition Structures (Å)

system	distance (Å)	PBE/DNP thermal	PBE/DNP Fermi	PBE/6-311G(d,p)
$[Al_{12}Mg\cdots H_2]^{\neq}$	$d(Al^1-H^1)$	1.707	1.701	1.707
	$d(Al^2-H^2)$	1.884	1.890	1.883
	$d(H^1-H^2)$	1.131	1.142	1.152
$[Al_{13}\cdots H_2]^{\neq}$	$d(Al^1-H^1)$	1.731	1.725	1.729
	$d(Al^2-H^2)$	1.940	1.960	1.957
	$d(H^1-H^2)$	1.051	1.056	1.066
$[Al_{12}Si\cdots H_2]^{\neq}$	$d(Al^1-H^1)$	1.736	1.736	1.740
	$d(Al^2-H^2)$	2.058	2.060	2.062
	$d(H^1-H^2)$	1.133	1.134	1.135

In this section, we present a brief assessment of the performance of PBE/DNP with and without the inclusion of thermal occupations against our secondary benchmark level, PBE/6-311G(d,p), for the evaluation of transition structures for dissociative adsorption of H_2 on the neutral X-centered $Al_{12}X$ clusters (X = Mg, Al, Si). These systems are representative of the reaction of triplet ($Al_{12}Mg$),[38,39] doublet (Al_{13}), and singlet ($Al_{12}Si$) clusters with H_2. We have identified two possible types of transition structure for these processes, which can be described as bridge and hollow structures (Figure 1). In both of these transition structures, one hydrogen atom is dissociating toward the atop position of the nearest aluminum atom, whereas, as the names imply, the second hydrogen atom is located approximately in bridge and hollow positions, respectively. We do not rule out the possibility that other pathways to dissociative adsorption of H_2 onto the clusters exist. Figure 1 displays the main features of hollow and bridge transition structures with identification of the key atoms described in Table 1.

It is clear from Table 1 that there is generally very close agreement in the key transition structure distances for all three levels. Interestingly, the inclusion of thermal occupation at the 0.136 eV level is generally found to have a negligible effect on these key distances. This differs from our observations for the isolated clusters where the inclusion of thermal occupations was found to eliminate Jahn−Teller distortions resulting in the shortening of some bonds and an increase in symmetry.

Table 2 presents reaction barriers ($\Delta H^{\neq}$) and enthalpies (ΔH) for the reaction of H_2 with $Al_{12}Mg$, Al_{13}, and $Al_{12}Si$ respectively at the PBE/DNP level with and without thermal occupations and compared against the benchmark G3(MP2)-RAD level.

TABLE 2: Effects of Thermal Occupations on Reaction Energies (eV) of $Al_{12}X/H_2$ Systems

system	property	PBE/DNP Thermal	PBE/DNP Fermi	G3(MP2)-RAD
$[Al_{12}Mg\cdots H_2]^{\neq}$	$\Delta H^{\neq}$	0.525	0.219	0.447
	ΔH	−0.410	−0.540	−0.422
$[Al_{13}\cdots H_2]^{\neq}$	$\Delta H^{\neq}$	0.797	0.539	0.976
	ΔH	−0.043	−0.285	0.047
$[Al_{12}Si\cdots H_2]^{\neq}$	$\Delta H^{\neq}$	1.368	1.375	1.798
	ΔH	+0.238	+0.240	0.617
MAD	$\Delta H^{\neq}/\Delta H$	0.229/0.159	0.362/0.274	
MD	$\Delta H^{\neq}/\Delta H$	−0.117/−0.151	−0.362/−0.274	

Previously,[35] we found that the PBE/DNP and PBE/6-311G(d,p) levels gave close agreement with a modified form of the high-level G3(MP2)-RAD benchmark level for binding energies, ionization potentials and electron affinities of Al_{13} and $Al_{12}Si$ clusters and the H binding energies for $Al_{12}XH_n$ (X = Al or Si, n = 1 or 2). We also found that the thermal occupations procedure generally lowers the energy of open-shell species relative to closed-shell species contributing to slightly poorer performance for binding energies, ionization energies, and electron affinities, which require the determination of the difference in energy of closed- and open-shell species. However, as we can see from the mean absolute deviations in Table 2, the PBE/DNP(Thermal) level actually provides closer agreement with G3(MP2)-RAD than standard PBE/DNP for both reaction barriers and enthalpies. Inspection of the data reveals that the binding energy for closed-shell H_2 is significantly underestimated by PBE/DNP (−0.257 eV), regardless of the inclusion thermal occupations. Therefore, the overestimation of the binding energy of open-shell $Al_{12}X$ by PBE/DNP(Thermal) is generally canceled by the underestimation of the binding energy of H_2, whereas for standard PBE/DNP, where the binding energies of the clusters are only slightly underestimated, the errors add together. Consequently, PBE/DNP systematically underestimates the barriers and enthalpies for these reactions relative to G3(MP2)-RAD, whereas at PBE/DNP(Thermal) the errors are somewhat more random depending on the multiplicity of $Al_{12}X$. We would therefore recommend that for investigation of chemisorption of H_2 on larger Al_n clusters where the G3(MP2)-RAD procedure may not be computationally feasible, that the standard PBE/DNP level be used with the addition of a correction of +0.36 eV to barriers and +0.27 eV to enthalpies. For the remainder of this study, we will provide both PBE/DNP and G3(MP2)-RAD energies.

B. Transition Structure Geometries. Key distances of the transition structures for hydrogen dissociation on charged and neutral $Al_{12}X$ clusters, calculated at the PBE/6-311G(d,p) level, are presented in Table 3. Overall, the shortest transition structure distances are generally observed for the $Al_{12}Mg$-based systems, whereas the values for the Al_{13} and $Al_{12}Si$ systems are longer and tend to span a smaller range. As we noted in the previous section, two possible types of transition structures are possible for these systems; however, we were only able to locate both bridge and hollow transition structures for the neutral Al_{13}/H_2 system. For the remaining systems, there is a preference for hollow-type transition structures for the positively charged systems (Al_{13}^+ and $Al_{12}Si^+$), whereas for the remaining systems, bridge-type transition structures are favored. Because it is difficult to compare directly the distances of the hollow and bridge type TSs, due to the different geometric requirements of these structures, we discuss each group separately.

First, we consider the hollow TS structures, and interestingly we find that, whereas the 37 valence electron $Al_{12}Mg^+$ system has the shortest Al^1-H^1 distance, the 38 valence electron Al_{13}^+ system has the longest value, with the value for $Al_{12}Si^+$ intermediate between these extremes. In comparison, the Al^2-H^2 distances exhibit the opposite trend with the Al_{13}^+/H_2 system having the shortest value and $Al_{12}Mg^+/H_2$ and $Al_{12}Si^+/H_2$ having significantly longer values. The H^1-H^2 distances generally decrease with the number of valence electrons.

TABLE 3: Geometric Parameters of Neutral and Charged $Al_{12}X/H_2$ (X = Al, Si, Mg) Transition Structures and Products (Å) at the PBE/6-311G(d,p) Level

system	$d(Al_1-H_1)$ (Å)	$d(Al_2-H_2)$ (Å)	$d(Al_2-H_2)$ (Å)
Association Complex			
Al_{13}^+/H_2	2.443	2.583/2.689	0.784
Transition Structures			
$[Al_{12}Mg^+\cdots H_2]^{\neq}$ hollow [a]	1.699	2.047/2.219	1.199
$[Al_{12}Mg\cdots H_2]^{\neq}$ bridge	1.707	1.883	1.152
$[Al_{12}Mg^-\cdots H_2]^{\neq}$ bridge	1.750	1.991	1.054
$[Al_{13}^+\cdots H_2]^{\neq}$hollow	1.802	1.992/1.992	1.087
$[Al_{13}\cdots H_2]^{\neq}$ bridge	1.729	1.957	1.066
$[Al_{13}\cdots H_2]^{\neq}$ hollow	1.728	2.164/2.164	1.086
$[Al_{13}^-\cdots H_2]^{\neq}$bridge	1.763	2.085	1.087
$[Al_{12}Si^+\cdots H_2]^{\neq}$hollow	1.728	2.134/2.135	1.069
$[Al_{12}Si\cdots H_2]^{\neq}$bridge	1.740	2.062	1.135
$[Al_{12}Si^-\cdots H_2]^{\neq}$bridge	1.757	1.952	1.201
Product			
$Al_{12}MgH_2^+$ (A1B1,2)	1.592	1.741/1.832	2.753
$Al_{12}MgH_2$ (A1B1,2)	1.599	1.744/1.857	2.772
$Al_{12}MgH_2^-$ (A1A2)	1.615	1.712	2.639
$Al_{13}H_2^+$ (A1B2,2)	1.593	1.806/1.805	3.263
$Al_{13}H_2$ (A1B1,2)	1.602	2.639	1.721
$Al_{13}H_2$ (A1H1,2,2)	1.601	1.916/1.916	2.739
$Al_{13}H_2^-$ (A1A2)	1.614	1.614	3.272
$Al_{12}SiH_2^+$ (A1H1,2,2)	1.596	1.902/1.902	2.713
$Al_{12}SiH_2$ (A1H2,2,3)	1.611	1.670	5.494
$Al_{12}SiH_2^-$ (A1A2)	1.628	1.628	4.730

[a] Transition structure contains second imaginary frequency (−45 cm^{-1}).

For the neutral bridge systems, the Al^1-H^1 and Al^2-H^2 distances increase with the number of cluster valence electrons but the H^1-H^2 distances do not follow this trend. Interestingly, the reverse seems to be true for the negatively charged systems, with a gradual increase in the H^1-H^2 distance with the number of cluster valence electrons but no clear trend for the Al^1-H^1 and Al^2-H^2 distances.

We note that generally the Al^1-Al^2 distances in the transition structures are longer than in the bare clusters indicating that during the reaction there is a distortion of the cluster geometry.

We compare these results with the study of Hammer et al.[3] who investigated the full minimum energy pathway for the H_2 molecule to absorb and dissociate on an Al(110) surface using a Car/Parrinello LDA approach. They found that the H_2 molecule dissociates from a fairly open long bridge site with $d(H^1-H^2) \sim 1.3$ Å, which is somewhat longer than our values for the cluster-based reactions. They also found that for a (1 × 1) overlayer of atomic hydrogen chemisorbed on the Al(110) surface, the most stable location for the hydrogen atoms is the atop positions. Similarly, for our systems we find that the bridge transitions structures generally lead to the atop(1)−atop(2) (A1A2) or atop(1)−bridge(1,2) (A1B1,2) isomers of $Al_{12}XH_2$ (part c of Figure 1). The only exception to this is the neutral $Al_{12}Si$ system for which the product is the atop(1)−hollow(2,2,3) isomer (A1H2,2,3).[40] The hollow-type transition structures generally lead to atop(1)−hollow(1,2,2) (A1H1,2,2) or atop(1)−bridge(2,2) (A1B2,2) isomers of $Al_{12}XH_2$.

Cui et al.[27] reported that under their experimental conditions D_2 is physisorbed on the closed-shell Al_{13}^- rather than forming the $Al_{13}H_2^-$ dihydride. Therefore, we attempted to locate local minima corresponding to the physisorbed Al_{13}^-/H_2 adduct.

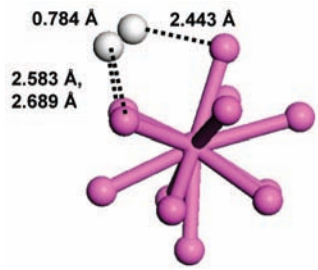

Figure 2. Association complex for the Al_{13}^+/H_2 system.

TABLE 4: Reaction Energies for $Al_{12}X/H_2$ Systems (eV) at the PBE/DNP (in Parentheses) and G3(MP2)-RAD Level

system	$\Delta H^{\neq(\text{forward})}$	$\Delta H^{\neq(\text{reverse})}$	ΔH
$[Al_{12}Mg^+\cdots H_2]^{\neq}$	(0.231)	(0.856)	(−0.624)
	0.598[a]	0.971[a]	−0.373[a]
$[Al_{12}Mg\cdots H_2]^{\neq}$	(0.219)	(0.759)	(−0.540)
	0.447	0.869	−0.422
$[Al_{12}Mg^-\cdots H_2]^{\neq}$	(0.640)	(1.139)	(−0.500)
	1.061	1.109	−0.048
$[Al_{13}^+\cdots H_2]^{\neq}$	(−0.445)	(0.541)	(−0.986)
	0.081	0.579	−0.498
$[Al_{13}\cdots H_2]^{\neq bridge}$	(0.539)	(0.824)	(−0.285)
	0.976	0.929	0.047
$[Al_{13}\cdots H_2]^{\neq hollow}$	(0.536)	(0.878)	(−0.341)
	0.969	0.979	−0.010
$[Al_{13}^-\cdots H_2]^{\neq}$	(1.342)	(1.136)	(0.206)
	1.770	1.178	0.592
$[Al_{12}Si^+\cdots H_2]^{\neq}$	(0.591)	(0.830)	(−0.239)
	1.010	0.910	0.099
$[Al_{12}Si\cdots H_2]^{\neq}$	(1.375)	(1.135)	(0.240)
	1.798	1.181	0.617
$[Al_{12}Si^-\cdots H_2]^{\neq}$	(1.040)	(1.329)	(−0.289)
	1.574	1.548	0.025

[a] PBE/DNP corrected value.

Similarly, we tried to locate stable H_2 adduct structures for each of the clusters in our study. However, the only system for which we could identify a stable H_2 adduct structure on the PBE/DNP and PBE/6-311G(d,p) potential-energy surfaces was for the Al_{13}^+/H_2 system (Figure 2). This is surprising in light of the fact that Al_{13}^+ was the only cluster cation for which Jarrold and Bower[26] did not experimentally identify the formation of an adduct. Alternatively, they note that the main product of the reaction of D_2 with Al_{13}^+ is $Al_{13}D^+$. We will discuss this aspect further in the next section. The fact that we were unable to identify $Al_{12}XH_2$ adducts for the remaining systems, in particular Al_{13}^-, may indicate the need to use a procedure that better describes dispersion-type interactions, which will be significant in these species.

C. Comparison of Reaction Barriers and Enthalpies for $Al_{12}X/H_2$ systems. Forward and reverse reaction barriers and reaction enthalpies calculated at PBE/DNP (in parentheses) and G3(MP2)-RAD levels are presented in Table 4. As noted in section 3A, PBE/DNP underestimates the binding energy of H_2 and therefore systematically underestimates the barriers and enthalpies for these reactions; however, we provide these values in Table 4 for comparison. In the text, we will predominantly discuss the high-level G3(MP2)-RAD values.

The first point to note from Table 4 is that the barrier for dissociation of H_2 on Al_{13}^+ is calculated as 0.081 eV; however, as indicated in the previous section, we have identified an association complex for Al_{13}^+/H_2 system, and this adduct is 0.074 eV lower in energy than the isolated reactants and the subsequent barrier for H_2 dissociation from this complex is 0.155 eV.[41] The next lowest forward barrier for these systems is

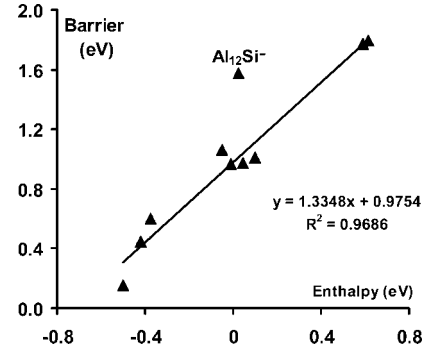

Figure 3. Plot of barrier height versus reaction enthalpy.

predicted for the isoelectronic $Al_{12}Mg/H_2$ system. Interestingly, both Al_{13}^+ and $Al_{12}Mg$ have 38 valence electrons, and the addition of H_2 to the cluster should lead to a very stable 40 electron closed-shell configuration, and in fact these systems are also predicted to have the largest exothermicities of all of the systems considered. In comparison, the forward barriers for the 39 electron systems ($Al_{12}Mg^-$, Al_{13}^{bridge}, Al_{13}^{hollow}, and $Al_{12}Si^+$) are considerably higher and cover only a narrow range (0.969−1.061 eV). It is also interesting to note that the forward barriers for the bridge and hollow pathways of the Al_{13}/H_2 system are very similar. The enthalpies for the 39 electron systems also show a small variation in values from the slightly exothermic $Al_{12}Mg^-$ system (−0.048 eV) through to the slightly endothermic $Al_{12}Si^+$ system (+0.099 eV). For the closed-shell 40-electron systems (Al_{13}^- and $Al_{12}Si$), there is a further increase in the barrier heights, and both of these reactions are also predicted to be significantly endothermic (+0.592 and +0.617 eV, respectively). Moving on to the 41-electron $Al_{12}Si^-$ system, the barrier is also predicted to be quite high but slightly lower than that of 40-electron systems. Interestingly, this reaction is almost energy neutral, with a reaction enthalpy of only +0.025 eV. For the 37-electron $Al_{12}Mg^+$ system, we were unable to obtain a G3(MP2)-RAD energy for the $Al_{12}Mg^+$ cluster, therefore we report a corrected PBE value. These results suggest that there is some correlation in the reactivity of these clusters with the predictions of the Jellium model.

In Figure 3, we plot the barrier heights versus reaction enthalpies. Nine of the points in this plot lie on a line of best fit with an $R^2 = 0.9686$ indicating a very strong Bell−Evans−Polanyi[42] type correlation between barrier height and reaction enthalpy for these closely related systems. If the remaining point is included in the regression analysis, the R^2 value falls to 0.8581. The first point to note from this plot is the fact that these systems are largely driven by thermodynamics. Second, 9 of the 10 systems are closely related within the Jellium model by the fact that they have a filled or nearly filled 2p valence Jellium orbital. However, the outlier occurs for the $Al_{12}Si^-$, which has a partially filled 1g valence Jellium orbital and therefore differs from the other systems.

Cox et al.[13] found experimentally that chemisorption of D_2 on neutral Al_{13} was extremely slow, such that the rate constants at room temperature are effectively zero. Despite our calculations indicating that there are two separate pathways to $Al_{13}H_2$, the barriers for both of these processes are quite high, in agreement with the experimental results. However, when they added D_2 directly to the helium carrier gas (which enables D_2 decomposition), then product peaks were observed for $Al_{13}H_n$ ($n = 1-3$). This is in agreement with our previous study[35] that demonstrated that there is no barrier for the addition of 1 or 2 H atoms to the Al_{13} cluster and that the binding of the H atoms is quite strong.[43] In the theoretical study of H_2 chemisorption

TABLE 5: Partial Atomic Charges[a]

	$\Delta H^{\neq}$	X	Al^1	H^1	H^2	Al^2 ($Al^{2'}$)
$Al_{12}Mg^+$		−0.034	+0.078 − +0.091			
$[Al_{12}Mg^+\cdots H_2]^{\neq}$	0.598[b]	−0.240	+0.146	−0.035	+0.035	+0.141 (+0.100)
$Al_{12}Mg$		−0.147	−0.049 − +0.025			
$[Al_{12}Mg\cdots H_2]^{\neq}$	0.447	−0.274	+0.072	−0.117	+0.052	+0.065
$Al_{12}Mg^-$		−0.257	−0.031 − −0.093			
$[Al_{12}Mg^-\cdots H_2]^{\neq}$	1.061	−0.253	+0.069	−0.165	+0.080	−0.088
Al_{13}^+		−0.438	+0.110 − +0.130			
$[Al_{13}^+\cdots H_2]^{\neq}$	0.081	−0.513	+0.172	−0.034	−0.042	+0.133 (+0.133)
Al_{13}		−0.452	+0.034 − +0.041			
$[Al_{13}^{bridge}\cdots H_2]^{\neq}$	0.976	−0.410	+0.109	−0.123	+0.070	+0.020
$[Al_{13}^{hollow}\cdots H_2]^{\neq}$	0.969	−0.420	+0.101	−0.114	−0.049	+0.020 (+0.019)
Al_{13}^-		−0.469	−0.044			
$[Al_{13}^-\cdots H_2]^{\neq}$	1.770	−0.419	+0.040	−0.257	+0.161	−0.119
$Al_{12}Si^+$		−0.627	+0.134 − + 0.137			
$[Al_{12}Si^+\cdots H_2]^{\neq}$	1.010	−0.557	+0.178	−0.087	+0.048	+0.120 (+0.120)
$Al_{12}Si$		−0.576	+0.048			
$[Al_{12}Si\cdots H_2]^{\neq}$	1.798	−0.535	+0.071	−0.239	+0.187	−0.021
$Al_{12}Si^-$		−0.473	−0.036 − −0.084			
$[Al_{12}Si^-\cdots H_2]^{\neq}$	1.574	−0.488	+0.084	−0.225	+0.005	−0.028

[a] Atom labels as show in Figure 1. X = core atom of cluster. [b] PBE/DNP corrected value.

on the Al(110) surface, Hammer and co-workers[5] obtained a barrier height of 0.25 eV with LDA and 0.54 and 0.70 eV for GGA with different supercells respectively, which may indicate intermolecular H−H interactions due to periodic boundary conditions. These values are somewhat lower than our G3(MP2)-RAD values for the Al_{13}/H_2 cluster systems.

As noted earlier, Jarrold and Bower[26] found that adsorption of D_2 onto Al cluster cations occurred in the ion beam for all clusters in the size range of Al_8^+ to Al_{27}^+, except for Al_{13}^+, and that these adducts arise from single collisions. Further to this, they indicate that the main product of the reaction of Al_n^+ ($n > 12$) with D_2 is Al_nD^+ rather than $Al_nD_2^+$. In comparison, we find that the formation of an association complex (adduct) is an energetically favorable process, and the barrier to dissociative adsorption of H_2 onto the cluster from this complex is quite small. Therefore, the fact that $Al_{13}H_2^+$ (or $Al_{13}D_2^+$) is not observed experimentally suggests that either an alternative lower-energy reaction occurs to produce $Al_{13}D^+$ or that the $Al_{13}D_2^+$ species is only an intermediate that subsequently undergoes further rapid reaction or decomposition.

Cui et al.[27] investigated $Al_nD_2^-$ ($n = 3, 6-15$) anions using photoelectron spectroscopy, and their results suggest that for the closed-shell Al_{13}^-, D_2 is physisorbed onto the cluster rather than chemisorbed. Our calculations clearly indicate that there is a large barrier to dissociative adsorption of H_2 onto Al_{13}^-, which is in agreement with the experimental results. However, as noted earlier, we were unable to locate any stable structures on the potential energy surface corresponding to H_2 physisorbed on the cluster.

D. Electronic and Orbital Analysis. We begin our detailed analysis of these systems by first considering changes in the partial atomic charges. Table 5 presents atomic polar tensor (APT) partial atomic charges on key atoms of the bare clusters and the transition structures for each system.

First, we note that, for the neutral clusters, the central atom always carries a negative partial atomic charge and that the magnitude of this charge increases with the electronegativity of the core atom. Naturally, the charge is balanced by an even distribution (within each symmetry) of positively charged cage atoms. When we consider the cluster cations, we find that for $Al_{12}Mg^+$ there is a significant decrease in the charge of the core atom and it increases in the positive charges of the cage atoms. However, for Al_{13}^+ and $Al_{12}Si^+$, while there are increases in the positive charges of the cage atoms, there is only a slight decrease in the charge of the core atom of Al_{13}^+, and for $Al_{12}Si^+$ there is in fact an increase in the negative charge on Si. For the negatively charged $Al_{12}Mg^-$, there is an increase in the negative charge on Mg, and the cage atoms also adopt a slight negative charge. For Al_{13}^-, there is only a slight increase in the negative charge on the core Al but all of the cage Al atoms become negatively charged, whereas for $Al_{12}Si^-$ there is actually a decrease in charge on Si while again the cage aluminums adopt negative charges. These trends reflect the significant differences in electronic environments brought about by the change in electronegativity of the core atom, with electronegative Si generally drawing greater charge from the cage Al atoms and electropositive Mg generally donating greater charge to the cage atoms for the same overall cluster charge.

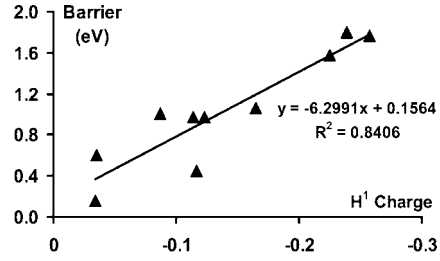

Figure 4. Plot of barrier height versus H^1 partial atomic charge.

For the transition states, there is generally a polarization of charge across both the cluster and the H_2 molecule. In particular, Al^1 always adopts a partial positive charge regardless of the overall charge state of the cluster. Similarly, H^1 always carries a partial negative charge in the transition structures. Generally, H^2 is positive and the magnitude of the charge on H^2 is smaller than that on H^1. However, for the Al_{13}^+ and Al_{13}^{hollow} systems, H^2 carries a small negative charge. The charge on Al_2 varies significantly in both sign and magnitude across the 10 systems.

We also note that there appears to be a correlation between the magnitude of the charge on H^1 and the reaction barriers as shown in Figure 4. This indicates that, in addition to the thermodynamic driving factors described in the previous section, the degree of charge transfer also makes an important contribution to the barrier height in these sytems.

These observations compare favorably with the study of Hammer et al.,[3−5] who found that the dipole moment of H_2 as

TABLE 6: Reaction Barriers and Energies of Frontier Orbitals (eV)

	$\Delta H^{\neq}$	HOMO	LUMO	$Al_{12}X^{HOMO}-H_2^{LUMO}$	$H_2^{HOMO}-Al_{12}X^{LUMO}$
$Al_{12}Mg^+/H_2$	0.598[a]	−8.269	−6.740	9.922	3.582
$Al_{12}Mg/H_2$	0.447	−4.911	−3.474	6.564	6.848
$Al_{12}Mg^-/H_2$	1.061	−1.679	−0.302	3.332	10.020
Al_{13}^+/H_2	−0.137	−8.533	−8.137	10.186	2.185
Al_{13}/H_2	0.976	−5.129	−3.373	6.782	6.949
Al_{13}^-/H_2	1.770	−1.968	−0.054	3.621	10.268
$Al_{12}Si^+/H_2$	1.010	−8.588	−6.587	10.241	3.735
$Al_{12}Si/H_2$	1.798	−5.205	−3.159	6.858	7.163
$Al_{12}Si^-/H_2$	1.574	−0.461	−0.019	2.114	10.303

[a] PBE/DNP corrected value.

it approaches the Al(110) surface is seen to first increase and then level off and finally to change sign during the course of the reaction. The initial increase is due to an orthogonalization of the metal states to the bonding state of H_2, which causes the surface electrons to be repelled from the region occupied by the H_2 bonding electrons toward the surface and a net inward shift of electrons results. Closer to the surface, the dipole moment changes sign because there is charge being transferred from the surface to the antibonding orbital of H_2, which is associated with the breaking of the H−H bond. Finally, there is a large negative dipole moment in the final stage associated with the outshift of charge needed to form the covalent bond between the surface and the two H atoms.

Next, we focus on the energies of the frontier orbitals of the species involved in these reactions. As can bee seen from Table 6, the $Al_{12}X^{HOMO}-H_2^{LUMO}$ gap is consistently lower than the corresponding $H_2^{HOMO}-Al_{12}X^{LUMO}$ gap for the neutral and negatively charged cluster/H_2 interactions. This compares favorably with the theoretical study of Upton and co-workers[25] for the interaction of H_2 with Al_6, where they found that generally electron transfer from the HOMO of the cluster to the LUMO (σ^* orbital) of H_2 was slightly more important than the transfer from the H_2^{HOMO} (σ orbital) to the cluster LUMO. Transfer of electron density into the H_2^{LUMO} is an important contribution to the weakening of the H−H bond during the reaction. However, despite this observation for the Al_6/H_2 system, there does not appear to be a strong correlation between $Al_{12}X^{HOMO}-H_2^{LUMO}$ and the barrier heights for our systems. These results suggest that the frontier orbital interactions are not the major contributor to the activation barrier heights, also in agreement with Upton and co-workers.[24,25] For the positively charged systems, the $H_2^{HOMO}-Al_{12}X^{LUMO}$ gap is actually smaller than $Al_{12}X^{HOMO}-H_2^{LUMO}$.

The important finding of the Al_6/H_2 study was that the activation barrier is dominated by Pauli repulsion at large interaction distances, similar to the observations of Hammer et al.[3−5] for the Al(110)/H_2 system. The energy of the system rises because significant changes in the cluster populations (orthogonalization) are necessary to initially minimize repulsive interactions between the cluster and H_2 and then subsequently to enable formation of the new Al−H bonds. We note in the transition structures for a number of these systems that there is significant distortion of the $Al_{12}X$ clusters away from their ground-state symmetry particularly for systems with high activation barriers. In fact, if we plot the barrier heights versus the distortion energies of the clusters in the TSs (Figure 5) we find quite a reasonable correlation for 9 of the 10 systems. The one outlier occurs for the $Al_{12}Mg$ system for which our calculations suggest that a triplet singlet crossing also contributes to the energy

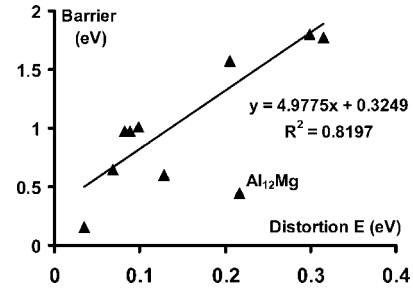

Figure 5. Plot of barrier height versus cluster distortion energy.

difference. However, the correlation for the majority of systems clearly indicates that the distortion of the cluster geometry, as a result of orthogonalization of the cluster orbitals with respect to H_2, makes a significant contribution to the barrier heights for these reactions.

4. Conclusions

The dissociative chemisorption of molecular hydrogen on charged and neutral aluminum clusters $Al_{12}X$ (X = Mg, Al, Si) was investigated using DFT and a modified G3(MP2)-RAD procedure. Reaction barriers ($\Delta H^{\neq}$) and enthalpies (ΔH) were determined for both neutral and singly charged clusters. The lowest barrier for dissociative adsorption of H_2 on a neutral cluster was found for the $Al_{12}Mg$ cluster, whereas the highest barrier was found to be on the closed-shell $Al_{12}Si$. The interaction of H_2 with Al_{13}^+ is found to proceed via an association complex, which is 0.07 eV lower in energy than the isolated species and from which the barrier to H_2 dissociative adsorption is only 0.16 eV. The most exothermic reaction of H_2 with $Al_{12}X$ occurs for the Al_{13}^+/H_2 system. In comparison, reactions with the closed-shell Al_{13}^- and $Al_{12}Si$ clusters are found to be slightly endothermic. These results indicate that there is some correlation between the reactivity of these clusters with H_2 and the predictions of the Jellium model. The barriers for H_2 desorption from the dihydrogenated clusters are generally quite substantial.

Whereas our calculations indicate that there are two separate dissociative adsorption pathways to $Al_{13}H_2$, the barriers for both of these processes are quite high, in agreement with the experimental results. For the Al_{13}^+/H_2 system, we find that the formation of an association complex (adduct) is an energetically favorable process, and the barrier to dissociative adsorption of H_2 onto the cluster from this complex is quite small. Therefore, the fact that $Al_{13}H_2^+$ (or $Al_{13}D_2^+$) is not observed experimentally suggests that either an alternative lower-energy reaction occurs to produce $Al_{13}D^+$ or that the $Al_{13}D_2^+$ species is only an intermediate that subsequently undergoes further rapid reaction or decomposition. Our calculations clearly indicate that there is a large barrier to dissociative adsorption of H_2 onto Al_{13}^-, which is in agreement with the experimental results. However, we were unable to locate any stable structures on the PBE/DNP or PBE/6-311G(d,p) potential energy surfaces corresponding to H_2 physisorbed on the cluster.

Importantly, our analysis of the reaction energetics indicates that these processes are largely controlled by thermodynamics. However, we have also determined that there are strong correlations between the degree of charge transfer in the transition state with the reaction barriers and also between the barriers and cluster distortion energies.

Acknowledgment. We gratefully acknowledge the award of an Australian Research Council Discovery Grant to carry out

this work. We also gratefully acknowledge allocation of computing time from the National Facility of the Australian Partnership for Advanced Computing (APAC).

References and Notes

(1) Sinke, G. C.; Walker, L. C.; Oetting, F. L.; Stull, D. R. *J. Chem. Phys.* **1967**, *47*, 2759–2761.

(2) Konovalov, S. K.; Bulychev, B. M. *Inorg. Chem.* **1995**, *34*, 172–175.

(3) Hammer, B.; Jacobsen, K. W.; Nørskov, J. K. *Phys. Rev. Lett.* **1992**, *69*, 1971–1974.

(4) Hammer, B.; Jacobsen, K. W.; Nørskov, J. K. *Surf. Sci.* **1993**, *297*, L68–L72.

(5) Gundersen, K.; Jacobsen, K. W.; Nørskov, J. K.; Hammer, B. *Surf. Sci.* **1994**, *304*, 131–144.

(6) Paul, J. *Phys. Rev. B* **1988**, *37*, 6164–6174.

(7) Sun, D.; Srinivasan, S. S.; Chen, G.; Jensen, C. M. *J. Alloys Compd.* **2004**, *373*, 265–269.

(8) Bogdanovic, B.; Schwickardi, M. *J. Alloys Compd.* **1997**, *253*−*4*, 1–9.

(9) Chaudhuri, S.; Muckerman, J. T. *J. Phys. Chem. B* **2005**, *109*, 6952–6957.

(10) Chaudhuri, S.; Graetz, J.; Ignatov, A.; Reilly, J. J.; Muckerman, J. T. *J. Am. Chem. Soc.* **2006**, *128*, 11404–11415.

(11) Rao, B. K.; Jena, P. *J. Chem. Phys.* **1999**, *111*, 1890–1904.

(12) Ahlrichs, R.; Elliott, S. D. *Phys. Chem. Chem. Phys.* **1998**, *1*, 13–21.

(13) Cox, D. M.; Trevor, D. J.; Whetten, R. L.; Kaldor, A. *J. Phys. Chem.* **1988**, *92*, 421–429.

(14) Taylor, K. J.; Pettiette, C. L.; Craycraft, M. J.; Chesnovsky, O.; Smalley, R. E. *Chem. Phys. Lett.* **1988**, *152*, 347–352.

(15) Knight, W. D.; Clemenger, K.; de Heer, W. A.; Saunders, W. A.; Chou, M. Y.; Cohen, M. L. *Phys. Rev. Lett.* **1984**, *52*, 2141–2143.

(16) Chou, M. Y.; Cohen, M. L. *Phys. Lett.* **1986**, *113A*, 420–424.

(17) Burkart, S.; Blessing, N.; Klipp, B.; Müller, J.; Ganteför, G.; Seifert, G. *Chem. Phys. Lett.* **1999**, *301*, 546–550.

(18) Kawamura, H.; Kumar, V.; Sun, Q.; Kawazoe, Y. *Phys. Rev. B* **2001**, *65*, 045406.

(19) Mañanes, A.; Duque, F.; Méndez, F.; López, M. J.; Alonso, J. A. *J. Chem. Phys.* **2003**, *119*, 5128–5141.

(20) Yarovsky, I.; Goldberg, A. *Mol. Simul.* **2005**, *31*, 475–481.

(21) Han, Y.-K.; Jung, J.; Kim, K. H. *J. Chem. Phys.* **2005**, *122*, 124319.

(22) Jung, J.; Han, Y.-K. *J. Chem. Phys.* **2006**, *125*, 064306.

(23) Goldberg, A.; Yarovsky, I. *Phys. Rev. B* **2007**, *75*, 195403.

(24) Upton, T. H. *Phys. Rev. Lett.* **1986**, *56*, 2168–2171.

(25) Upton, T. H.; Cox, D. M.; Kaldor, A. In *The Physics and Chemistry of Small Clusters*; Jena, P., Ed.; Plenum: New York, 1987.

(26) Jarrold, M. F.; Bower, J. E. *J. Am. Chem. Soc.* **1988**, *110*, 70–78.

(27) Cui, L.-F.; Li, X.; Wang, L.-S. *J. Chem. Phys.* **2006**, *124*, 054308.

(28) Koch, W.; Holthausen, M. C. *A Chemist's Guide to Density Functional Theory*; Wiley-VCH: Weinheim, 2000.

(29) Hehre, W. J.; Radom, L.; Schleyer, P. v. R.; Pople, J. A. *Ab Initio Molecular Orbital Theory*; Wiley: New York, 1986.

(30) (a) Delley, B. *J. Chem. Phys.* **1990**, *92*, 508. (b) Delley, B. *J. Chem. Phys.* **2000**, *113*, 7756.

(31) Frisch, M. J. ; Trucks, G. W.; Schlegel, H. B.; Scuseria, G. E.; Robb, M. A.; Cheeseman, J. R.; Montgomery, J. A., Jr.; Vreven, T.; Kudin, K. N.; Burant, J. C.; Millam, J. M.; Iyengar, S. S.; Tomasi, J.; Barone, V.; Mennucci, B.; Cossi, M.; Scalmani, G.; Rega, N.; Petersson, G. A.; Nakatsuji, H.; Hada, M.; Ehara, M.; Toyota, K.; Fukuda, R.; Hasegawa, J.; Ishida, M.; Nakajima, T.; Honda, Y. Kitao, O.; Nakai, H.; Klene, M.; Li, X.; Knox, J. E.; Hratchian, H. P.; Cross, J. B.; Bakken, V.; Adamo, C.; Jaramillo, J.; Gomperts, R.; Stratmann, R. E.; Yazyev, O.; Austin, A. J.; Cammi, R.; Pomelli, C.; Ochterski, J. W.; Ayala, P. Y.; Morokuma, K.; Voth, G. A.; Salvador, P.; Dannenberg, J. J.; Zakrzewski, V. G.; Dapprich, S.; Daniels, A. D.; Strain, M. C.; Farkas, O.; Malick, D. K.; Rabuck, A. D.; Raghavachari, K.; Foresman, J. B.; Ortiz, J. V.; Cui, Q.; Baboul, A. G.; Clifford, S.; Cioslowski, J.; Stefanov, B. B.; Liu, G.; Liashenko, A.; Piskorz, P.; Komaromi, I.; Martin, R. L.; Fox, D. J.; Keith, T.; Al-Laham, M. A.; Peng, C. Y.; Nanayakkara, A.; Challacombe, M.; Gill, P. M. W.; Johnson, B.; Chen, W.; Wong, M. W.; Gonzalez, C.; Pople, J. A. *Gaussian 03*, Rev. D.01; Gaussian, Inc., Wallingford CT, 2004.

(32) Werner, H.-J.; Knowles, P. J.; Lindh, R.; Schütz, M.; Celani, P.; Korona, T.; Manby, F. R.; Rauhut, G.; Amos, R. D.; Bernhardsson, A.; Berning, A.; Cooper, D. L.; Deegan, M. J. O.; Dobbyn, A. J.; Eckert, F.; Hampel, C. ; Hetzer, G. ; Lloyd, A. W.; McNicholas, S. J.; Meyer, W.; Mura, M. E. Nicklass, A.; Palmieri, P.; Pitzer, R.; Schumann, U.; Stoll, H.; Stone, A. J.; Tarroni, R.; Thorsteinsson, T. *MOLPRO*, version 2006.1; see http://www.molpro.net.

(33) Perdew, J. P.; Burke, K.; Ernzerhof, M. *Phys. Rev. Lett.* **1996**, *77*, 3865–3868.

(34) Fowler, J. E.; Ugalde, J. M. *Phys. Rev. A* **1998**, *58*, 383–388.

(35) Henry, D. J.; Varano, A.; Yarovsky, I. *J. Phys. Chem. A* **2008**, *112*, 9835–9844.

(36) Henry, D. J.; Sullivan, M. B.; Radom, L. *J. Chem. Phys.* **2003**, *118*, 4849–4860.

(37) Cioslowski, J. *J. Am. Chem. Soc.* **1989**, *111*, 8333–8336.

(38) Our theoretical calculations indicate that the $Al_{12}Mg$ cluster is a stable structure with D_{5d} symmetry, due to a Jahn−Teller distortion, and a binding energy of 29.62 eV, which exists in the $^3A_{1g}$ triplet electronic state, in contrast to the recent report of Lu et al. 39

(39) Lu, Q. L.; Jalbout, A. F.; Luo, Q. Q.; Wan, J. G.; Wang, G. H. *J. Chem. Phys.* **2008**, *128*, 224707.

(40) The atop(1)−atop(2) and atop(1)−bridge(1,2) isomers are both saddle points on the potential energy surface. The atop(1)−hollow(1,2,2) isomer is a local minimum but the IRC analysis does not link the transition state to this structure.

(41) In our previous study,35 we reported on the C_2 symmetric 3B triplet state of Al_{13}^+ due to computational limitations at the time. However, in this work we report reaction barriers and enthalpies relative to the slightly lower energy C1 singlet structure at all levels of theory.

(42) (a) Evans, M. G.; Gergely, J.; Seaman, E. C. *J. Polym. Sci.* **1948**, *3*, 866–879. (b) Evans, M. G. *Discuss. Faraday Soc.* **1947**, *2*, 271–279.

(43) There is also no barrier for the addition of the H atom to the $Al_{12}Si$ and $Al_{12}Mg$ clusters, and the binding of the H atoms is quite strong (1.77 and 2.36 eV, respectively).

JP809619Q